Nonlinear Neural Network-Based Mixture Model for Estimating the Concentration of Nitrogen Salts in Turbid Inland Waters Using Hyperspectral Imagery

Javier Plaza, Pablo Martínez, Rosa Pérez, Antonio Plaza, Carmen Cantero

Neural Networks and Signal Processing Group (GRNPS)
Computer Science Department, University of Extremadura
Avda. de la Universidad s/n,10.071 Caceres, SPAIN
Contact e-mail: jplaza@unex.es

ABSTRACT

The development of hyperspectral imaging instruments designed for water quality assessment, such as the DLR Reflective Optics System Imaging Spectrometer (ROSIS), has created a need for methods which are able to infer water quality parameters of turbid inland waters, and to use those parameters as indicators for water quality. It has been reported that the irradiance reflectance and, subsequently, the radiance collected by the sensor in such scenario is usually the result of an intimate mixture of sub-pixel components. As a result, the commonly used linear mixing model may not be appropriate to describe materials composition. In this work, we develop a nonlinear neural network-based algorithm for estimating water constituent concentrations, with special emphasis on the detection of chemical substances provided by agricultural and industrial sources. The proposed neural network architecture consists of a modified multi-layer perceptron (MLP) whose entries are determined by a linear function activation provided by a Hopfield neural network algorithm (HNN). The combined HNN/MLP supervised model has been used to estimate the concentration of water constituents by training the MLP with ground spectra of nitrogen salts, which are commonly used in extensive agricultural farms. Such spectra were collected using a Minolta spectro-photometer. The model was calibrated in our laboratory by using mixtures of water and nitrogen salt in different proportions. Hyperspectral images collected by the ROSIS imaging spectrometer over the Guadiloba reservoir in Cáceres, SW Spain, are also used in this study to estimate the concentration of nitrogen salts in turbid inland waters.

Keywords: Water quality assessment, Hyperspectral imagery, Nonlinear mixture modeling, Neural networks.

1. INTRODUCTION

Water covers nearly three quarters of the surface of the Earth in the form of oceans, rivers, lakes, snow and glaciers. As a result, water pollution represents a major enviromental problem. In partcular, inland water systems can be fresh or saline within continental and island boundaries. They include lakes, rivers, ponds, streams, groundwater, springs, cave waters, floodplains, as well as bogs, marshes and swamps, which are traditionally grouped as inland wetlands. Biodiversity of inland waters is a source of food, income and livelihood. Lakes and rivers are particularly valuable watersystems. The ecological value of many lakes and rivers has been deteriorated in part as a result of human behaviour. Many differents pollutants have contributed to this deterioration process. These pollutants can be categorized, according to their nature, in organic pollutants such as phenols, hydrocarbons and detergents which are commonly used for industrial purposes; mineral contaminants such as heavy metals, phosphorus, and others which can be easily found in nature in the form of viral particles.

Assessment of water quality has traditionally been accomplished by limmological methods and laboratory-based analyses of field samples. This has been demonstrated to be time consuming and expensive. On other hand, the limited number of field samples is often disputed to represent the overall characteristics of a vast water body[1]. In order to overcome the above limitations, hyperspectral remote sensing techniques have been investigated for their potential use in estimation of individual water quality parameters, bearing successful results in a wide range of applications[2-3].

Chemical and Biological Standoff Detection II, edited by James O. Jensen,
Jean-Marc Thériault, Proceedings of SPIE Vol. 5584 (SPIE, Bellingham, WA, 2004)
0277-786X/04/$15 · doi: 10.1117/12.579805

Specifically, satellite monitoring of inland and coastal waters is generally difficult because water color, an indicator of water quality, is caused by the absorption and scattering of sunlight and skylight by organic and inorganic matter in the water. In mid-ocean water, the only colorant is chlorophyll-bearing phytoplankton and its decay products. Therefore, it is relatively straightforward to deduce concentrations of ocean chlorophyll based on the optical properties of this single colorant. In the case of inland waters, the color of natural water adjacent to or surrounded by a land mass is determined not only by phytoplankton and decay products, but also by other colored substances. These include suspended sediments and dissolved organic matter that come from the land. By addressing the individual colours of the different components of the water, e.g. green chlorophyll, red clay, and tea-coloured dissolved organic matter, a simple mixing paint-based model can be developed to calculate how much of each constituent must be present in the mixture to produce the color measured by the satellite. It has been reported that the irradiance reflectance and, subsequently, the radiance collected by the sensor in an inland water analysis scenario is usually the result of an intimate (nonlinear) mixture of sub-pixel components. As a result, the commonly used linear mixing model may not be appropriate to describe materials composition.

Neural networks have been widely used in remote sensing to estimate biophysical parameters from remotely sensed hyperspectral data via nonlinear procedures. In previous work, neural networks have been successfully applied for the purpose of estimating optically active constituent concentrations in the water from data adquired by passive sensors in the visible and near-infrared[4-7]. Most of the considered approaches are very sensitive to the training stage, which has to be accomplished using a variety of carefully selected field samples. In this work, we propose a completely automated neural network-based methodology for inferring the abundance of water pollutants in multi/hyperspectral scenes. The proposed neural network architecture consists of a modified multi-layer perceptron (MLP) whose entries are determined by a linear function activation provided by a Hopfield neural network algorithm (HNN). The network is trained by using pure spectral constituents (endmembers). By means of the training procedure above, the network is able to estimate the abundance fractions of endmembers in nonlinear fashion, thus adapting to the nonlinear mixing scenario that generally occurs in water analysis problems. Two different approaches are explored to generate the training samples: 1) manual selection of endmembers; and 2) automated identification of endmembers by our custom-designed automated morphological endmember extraction (AMEE) method.

The remainder of the paper is organized as follows. Section 2 presents an overview of the automated endmember extraction algorithm used in experiments to generate samples that will be used to train a combined HNN/MLP neural network architecture, described in section 3. In section 4, quantitative results based on simulated and real datasets are discussed. Finally, section 5 concludes with some remarks and hints at plausible future research.

2. AUTOMATED MORPHOLOGICAL ENDMEMBER EXTRACTION (AMEE)

The algorithm used to generate training samples for the proposed neural network architecture is the automated morphological endmember extraction (AMEE) algorithm. It is the only available endmember extraction algorithm that makes simultaneous use of spatial and spectral information via multi-channel morphological processing[8]. The input to the AMEE method is the full image data cube, with no previous dimensionality reduction. Let $\boldsymbol{h}$ denote the input hyperspectral data cube and $\boldsymbol{h}(x, y)$ denote the pixel vector at spatial location (x, y). Similarly, let K be a kernel defined in the spatial domain of the image (the x-y plane). This kernel, usually called structuring element (SE) in mathematical morphology terminology, is translated over the image. The SE acts as a probe for extracting or suppressing specific structures of the image objects, according to the size and shape of the SE. Having the above definitions in mind, the AMEE method is based on the application of multi-channel erosion and dilation operations to the data. The above operations are respectively defined as follows.

$$(\boldsymbol{h} \otimes K)(x, y) = \arg\_\,\mathrm{Min}_{(s,t)\in K} \left\{ \sum_s \sum_t \mathrm{dist}\big(\boldsymbol{h}(x, y), \boldsymbol{h}(x+s, y+t)\big) \right\} \quad (1)$$

$$(\boldsymbol{h} \oplus K)(x, y) = \arg\_\,\mathrm{Max}_{(s,t)\in K} \left\{ \sum_s \sum_t \mathrm{dist}\big(\boldsymbol{h}(x, y), \boldsymbol{h}(x-s, y-t)\big) \right\} \quad (2)$$

where dist is the spectral angle mapper (SAM)[8]. Multi-channel erosion (respectively, dilation) selects the pixel vector which minimizes (respectively, maximizes) a cumulative distance-based cost function, based on the sum of the SAM distance scores between each pixel in the spatial neighborhood defined by K and all the other pixels in the neighborhood. As a result, multi-channel erosion extracts the pixel vector that is more similar to its neighbors as opposed to multi-channel dilation, which extracts the most spectrally distinct pixel in the neighborhood (endmember candidate). It should be noted that, according to the definition of morphological erosion and dilation, the above operations are sensitive to the size and shape of the SE used in the computation. In our application, a morphological eccentricity index (MEI) is defined for each endmember candidate by calculating the SAM distance between the pixel provided by the dilation operation and the pixel provided by the erosion. This operation is repeated for all the pixels in the scene, using SE's with a range of different sizes, until a final MEI image is generated. Endmember selection is then accomplished by a fully automated approach which consists of two steps[8]: 1) Automated segmentation of the MEI image using Otsu's method; 2) Spatial/spectral region growing of resulting regions. A set of endmembers signatures $\{\boldsymbol{e}_{\mathrm{i}}\}_{\mathrm{i=1}}^{\mathrm{N}}$ is obtained as the final result of the algorithm.

3. NEURAL NETWORK ARCHITECTURE FOR THE NONLINEAR MIXING PROBLEM

Once a set of endmember signatures $\{\boldsymbol{e}_{\mathrm{i}}\}_{\mathrm{i=1}}^{\mathrm{N}}$ has been extracted by the AMEE algorithm, our goal is to solve the nonlinear mixing equation $\boldsymbol{h}(\mathrm{x},\mathrm{y}) = \sum_{\mathrm{i=1}}^{\mathrm{N}} c_{\mathrm{i}}\boldsymbol{e}_{\mathrm{i}}$ for each hyperspectral image pixel $\boldsymbol{h}(\mathrm{x},\mathrm{y})$. Let us denote by $\boldsymbol{e}_{\mathrm{i}} = [e_{1\mathrm{i}}, e_{2\mathrm{i}}, ..., e_{\mathrm{Li}}]^{\mathrm{T}}$ a pure endmember signature, where L is the number of spectral bands. Similarlu, let us denote by $c_{\mathrm{i}} = f(a_{\mathrm{i}})$ the contribution of endmember signature $\boldsymbol{e}_{\mathrm{i}}$ in the pixel given by an nonlinear mixing function f, where a_{i} is the real abundance fraction of $\boldsymbol{e}_{\mathrm{i}}$ in the pixel. If we express the problem using a matrix notation, i.e. $\boldsymbol{E} = [\boldsymbol{e}_1, \boldsymbol{e}_2, ..., \boldsymbol{e}_{\mathrm{N}}]$, $\boldsymbol{c} = [c_1, c_2, ..., c_{\mathrm{N}}]$ and $\boldsymbol{a} = [a_1, a_2, ..., a_{\mathrm{N}}]$, then our goal is to solve the equation $\boldsymbol{h}(\mathrm{x},\mathrm{y}) = \boldsymbol{E}\boldsymbol{c}^{\mathrm{T}}$ at each pixel[9]. In this work, we propose to solve the linear part of the problem, i.e. $\boldsymbol{c}^{\mathrm{T}} = \boldsymbol{E}^{-1}\boldsymbol{h}(\mathrm{x},\mathrm{y})$, by a modified Hopfield neural network (HNN). On other hand, the nonlinear part of the problem related with the mixing equation, i.e. $\boldsymbol{a} = f^{-1}(\boldsymbol{c})$, is solved by using a Multi-Layer Perceptron (MLP). The effectiveness of this approach has been demonstrated in previous work[10-12].

3.1 Modified Hopfield neural network (HNN)

In order to solve the first part of the equation, we use a modified Hopfield neural network (HNN) with gradient descent learning based on error minimization (see Fig. 1). The number of input neurons is N, i.e. the dimension of the fractional abundance vector $\boldsymbol{c}$. A weight matrix W is created by using the sample correlation matrix between AMEE-derived endmember materials $\{\boldsymbol{e}_{\mathrm{i}}\}_{\mathrm{i=1}}^{\mathrm{N}}$. The bias vector is dependent on the mixture spectrum under analysis. The proposed HNN is based on an iterative process where an initial abundance estimation $\boldsymbol{c}(\mathrm{t})$ is refined by multiplying $\boldsymbol{c}(\mathrm{t})$ by the weight matrix. The bias vector is then added and the result $\boldsymbol{c}(\mathrm{t}+1)$ is compared to that obtained at the previous iteration until a desired threshold condition is satisfied for convergence.

3.2 Multi-layer perceptron (MLP)

In order to solve the second part of the nonlinear mixing problem, we obtain the real fractional abundance map by means of the fractional contribution estimations provided by the HNN. For the above purpose, a Multi-layer perceptron (MLP) neural network is used. The entries to the MLP are the outputs of the HNN, which we denote by $\boldsymbol{c}_{(\mathrm{HNN})}$ (see Fig. 2). The number of input neurons is N, the same as the number of output neurons. The number of hidden neurons can be adjusted depending on the problem, and is only important in terms of convergence time. The training process is based on error back-propagation criteria, where the output nodes and the hidden nodes modify their respective weight matrices (V and

W) depending on a pre-defined error (delta), the input, and an adjustable learning parameter Alpha. The delta error of the output layer is calculated as the difference between the provided outputs and the desired outputs (ground truth fractional abundances), and this error is back-propagated to the hidden nodes until convergence is reached.

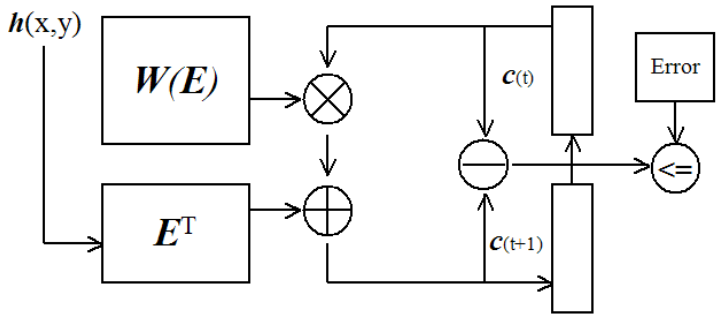

Figure 1. Schematic block diagram summarizing the performance of the HNN module.

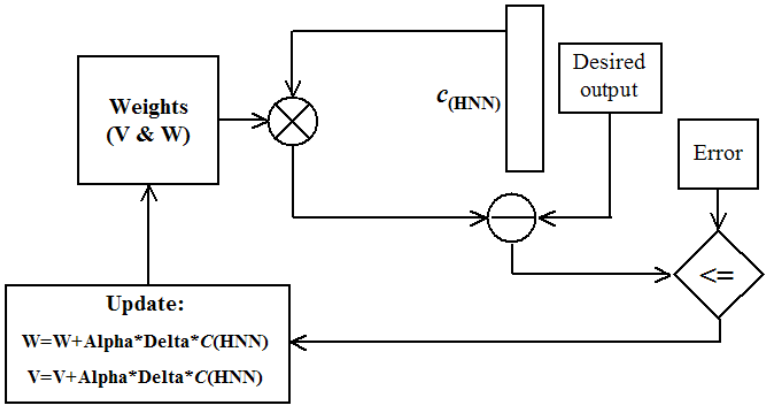

Figure 2. Schematic block diagram summarizing the performance of the MLP module.

4. EXPERIMENTAL RESULTS

Different experiments have been carried out in order to test the accuracy of the combined HNN/MLP neural network architecture in estimating the concentration of nitrogen salts in turbid inland waters. Our experiments can be divided into two different groups. Both linear and nonlinear simulated hyperspectral mixtures have been created for determining the performance of the neural algorithm. In both cases, a set of ground spectral samples were used. These data consist of 10 spectral samples collected in the laboratory using a Minolta 508d handheld spectrophotometer, which covers the spectral range from 0.4 μm to 0.7 μm. Real binary mixtures were created by mixing distilled water (composed by a saturated solution of water and fertilizers) with nitrogen salts in known proportions. These products were then mixed into several known volumes to produce the abundances displayed in Table 1.

Using the fractional abundances in Table 1, a simulated scene was constructed as follows[13]. The 110x110-pixel scene is formed by 11 vertical frames of 11-pixels width, and the abundances have been assigned to each frame so that the real mixtures between distilled water and nitrogen solution are arranged in progressive fashion, where the leftmost frame is made up with pure distilled water and the rightmost frame is composed of pure nitrogren solution. Figure 3(a) displays the 11 spectral signatures collected by the Minolta spectrophotometer, which comprise two pure spectral signatures (endmembers) and 9 binary mixtures as addressed in Table 1. For illustrative purposes, Figs. 3(b) and 3(c) respectively show the abundance fractions of the two endmembers, pure distilled water in Fig. 3(b) and pure nitrogen solution in Fig. 3(c). Finally, using the simulated image in Fig. 3, we have conducted a thorough investigation of the performance of different fractional abundance estimation methods, including: 1) the traditional linear mixture model (LMM); 2) the proposed HNN neural model alone, which is aimed at solving the mixture problem in linear fashion; and 3) the combined

HNN/MLP neural model, which is designed to solve the problem nonlinearly. Since the data used for experiments are real mixtures, it is expected that the mixing mechanism is highly nonlinear. In such case, it is of great interest to see which one of the approaches mentioned above provides the most accurate estimation results.

Abundance of distilled water	Abundance of nitrogen solution
100 %	0 %
90 %	10 %
80 %	20 %
70 %	30 %
60 %	40 %
50 %	50 %
40 %	60 %
30 %	70 %
20 %	80 %
10 %	90 %
0 %	100 %

Table 1. Abundances of binary mixtures made up with distilled water and a nitrogen solution.

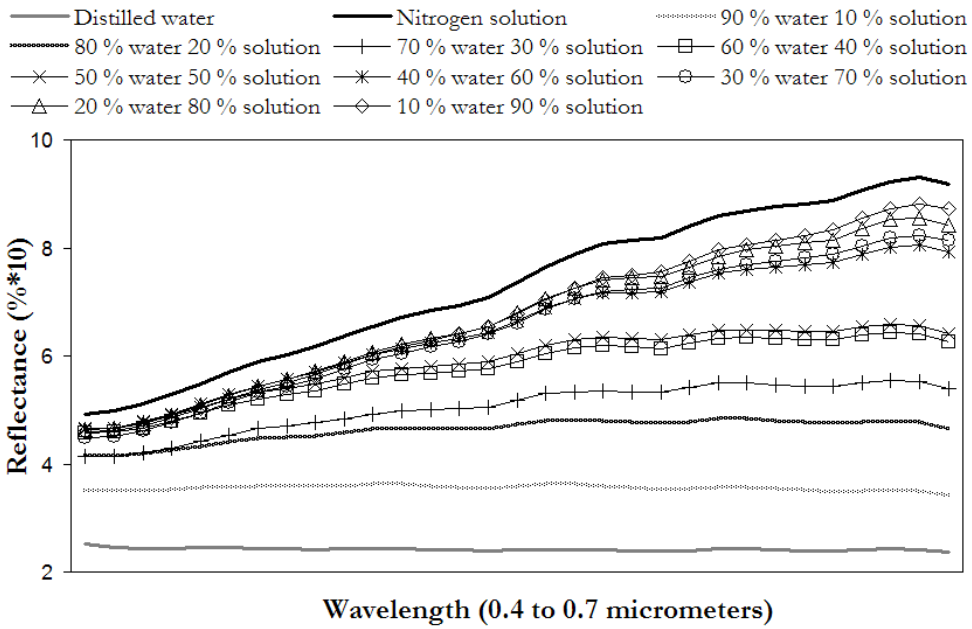

(a) Endmember spectra used in simulations.

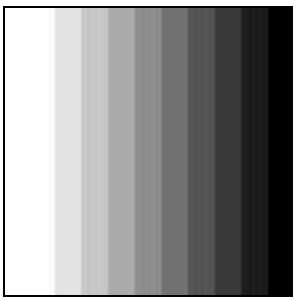

(b) Water abundance map

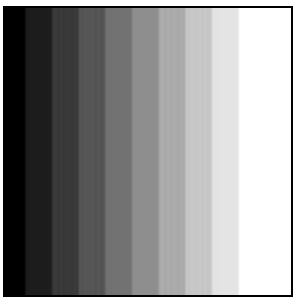

(c) Nitrogen abundance map

Figure 3. (a) Spectra of real pure and mixed samples of distilled water and nitrogen solution. (b) Abundance map of distilled water. (c) Abundance map of nitrogen solution.

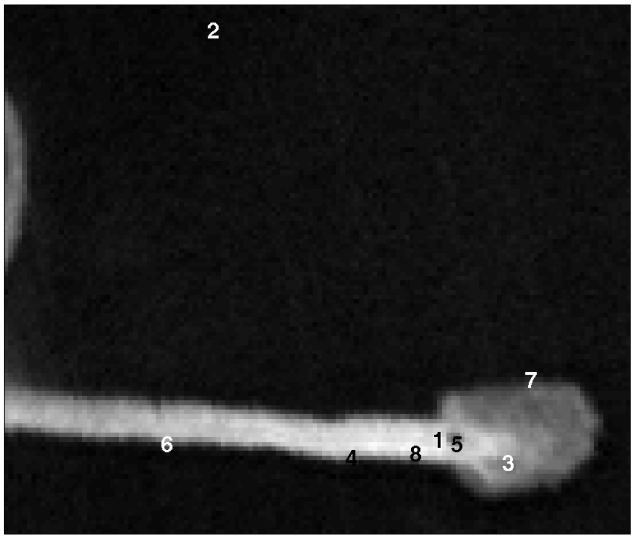

(a) Original image with endmember pixel locations

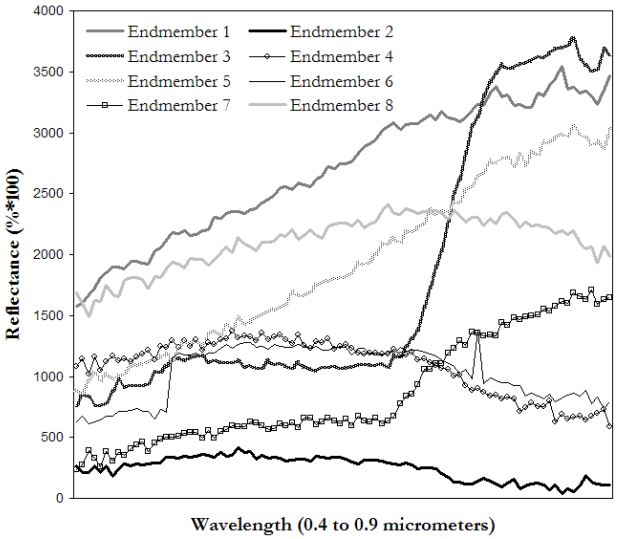

(b) AMEE-derived endmember signatures

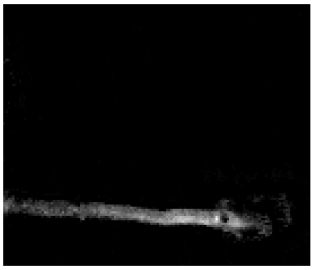

(c) Endmember 1 – soil/bridge

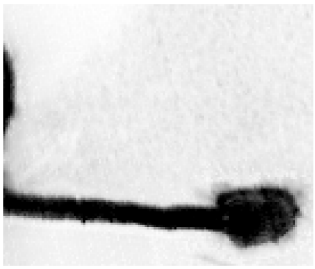

(d) Endmember 2 – pure water

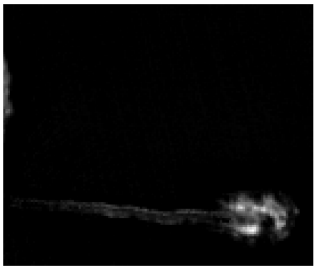

(e) Endmember 3 – grass

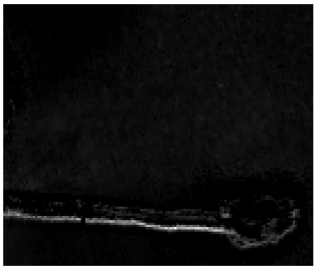

(f) Endmember 4 – possible pollutant

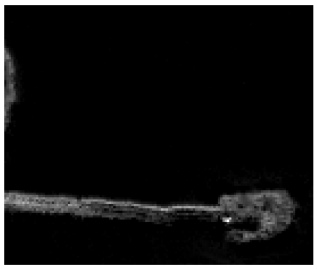

(g) Endmember 5 – anomaly

(h) Endmember 6 – anomaly

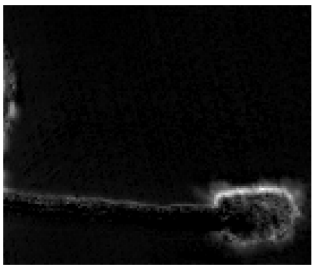

(i) Endmember 7 – playa

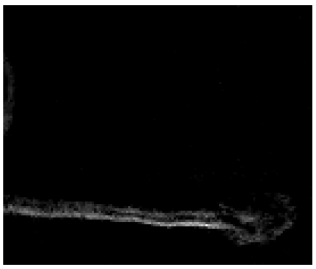

(j) Endmember 8 – possible pollutant

Figure 4. (a) Band at 547 nm of a ROSIS hyperspectral image over Guadiloba reservoir in Caceres, SW Spain. (b) AMEE-derived endmember pixels. (c-j) Fractional abundance maps associated to each of the AMEE-derived endmember pixels in (b).

Table 2 shows the abundance estimation results provided by LMM, HNN and HNN/MLP for the simulated image in Fig. 3. AMEE-derived endmembers were used as an input to the LMM. Also, AMEE endmembers were used to train the two considered HNN and HNN/MLP neural architectures. Finally, in order to study the impact of training samples on the proposed HNN/MLP, three additional training scenarios are tested. In the first one, denoted in Table 2 by HNN/MLP-2, only the two AMEE-derived endmembers are used for the training. In the second case, denoted by HNN/MLP-3, the two AMEE-derived endmembers plus a sample mixture made up with (50% water, 50% nitrogen) were used for the training. In the third case, denoted by HNN/MLP-5, the two AMEE-derived endmembers plus three additional sample mixtures, (50% water, 50% nitrogen), (70% water, 30% nitrogen) and (30% water, 70% nitrogen) were used for the training.

Finally, all 9 possible sample mixtures were used in addition to 2 endmembers for training, a scenario that is denoted by HNN/MLP-11 in the table.

	Abundance	LMM	HNN	HNN/MLP-2	HNN/MLP-3	HNN/MLP-5	HNN/MLP-11
	1	1	1	1	0.979723	0.909523	0.819258
	0.9	0.95794	1.036313	1.036302	1.015924	0.943020	0.848898
	0.8	0.898681	0.977146	0.977136	0.956940	0.888442	0.800604
	0.7	0.857185	0.961050	0.961040	0.940894	0.873594	0.787466
	0.6	0.783068	0.873993	0.873985	0.854114	0.793294	0.716408
Water	0.5	0.457624	0.555696	0.555694	0.536874	0.499734	0.456595
	0.4	0.440969	0.548043	0.548041	0.529247	0.492676	0.45048
	0.3	0.337385	0.477575	0.477575	0.459021	0.427691	0.392826
	0.2	0.171310	0.246902	0.246907	0.229165	0.214984	0.204529
	0.1	0.022466	0.019963	0.019971	0.003061	0.005744	0.019273
	0	0	0	0	0	0	0.002977
	1	1	1	1	1	1	0.994436
	0.9	1	0.980318	0.980326	0.995086	0.991993	0.978444
	0.8	1	0.756515	0.756519	0.772349	0.786235	0.796599
	0.7	1	0.527096	0.527096	0.543984	0.575138	0.609838
	0.6	1	0.456594	0.456593	0.473799	0.510229	0.552370
Nitrogen	0.5	1	0.448922	0.44820	0.466160	0.503164	0.546113
	0.4	0.338854	0.128165	0.128158	0.146797	0.207646	0.284242
	0.3	0.111732	0.039685	0.039676	0.058688	0.126062	0.211873
	0.2	0.068928	0.023290	0.023281	0.042360	0.110942	0.198456
	0.1	0	0	0	0	0.055229	0.149010
	0	0	0	0	0.019167	0.089461	0.179396

Table 2. Fractional abundance estimation results produced by the considered methods.

As shown in Table 2, the LMM only provides the best abundance estimation results sporadically, while in most of the cases the proposed HNN/MLP produces the most accurate results in terms of determining the concentration of distilled water and nitrogen solution in real nonlinear mixtures. This is particularly true when the considered HNN/MLP-5 and HNN/MLP-11 training scenarios are considered. For illustrative purposes, Table 3 shows root mean square error (RMSE) scores in the abundance estimation. As shown in Table 3, HNN/MLP-11 results in lower RMSE scores than any of the other methods. Although LMM sporadically produces accurate estimation results, it is clear from Table 3 that the overall performance of LMM is considerably lower than that of HNN when this neural model is used to solve the linear mixture problem. In addition, the proposed nonlinear HNN/MLP model is consistently better than the linear HNN. These results seem to indicate that a nonlinear model is required in order to estimate the concentration of nitrogen salts in turbid inland waters.

In order to investigate the performance of the proposed method in a real scenario, a preliminary study has been conducted using data collected by the DLR Reflective Optics System Imaging Spectrometer (ROSIS) over the Guadiloba reservoir in Caceres, SW Spain. The scene considered for experiments has a size of 115x136 pixels of 1.2 meters, and the spectral coverage is 90 bands from 0.4 μm to 0.9 μm. Fig. 4(a) shows the band at 547 nm of the original image, where a bridge and a small island in the middle of the reservoir are clearly visible. This figure also shows several numbers which correspond to the spatial locations of eight AMEE-derived endmember pixels for the scene. The spectral signatures of these pixels are shown in Fig. 4(b). Ground-truth data were collected during a test visit to the site at the same time as the image data collection by using an ASD FieldSpec Pro spectroradiometer. As part of our experiment, ground samples were compiled. These samples revealed the presence of organic pollutants at one side of the bridge. The purest water concentration is present in the upper area of the scene. Several anomalous pixels can also be visually identified. For illustrative purposes, Figs. 4(c-j) show the fractional abundance maps estimated for the eight endmembers in Fig. 4(b). The maps reveal a strong concentration of endmember signatures labeled with numbers 4 and 8 at one side of the bridge, which may be associated to water pollutants. Further work is still needed in order to extract more significant conclusions from the analysis of the ROSIS real hyperspectral data addressed in Fig. 4.

Mixture	LMM	HNN	HNN/MLP-2	HNN/MLP-3	HNN/MLP-5	HNN/MLP-11
Pure water (w)	0	0	0	0.00038	0.008	0.0324
Pure nitrogen (n)	0	0	0	0.00024	0.0001	0.00001
(90% w, 10% n)	0.0202	0.01868	0.01868	0.01365	0.00192	0.0025
(80% w, 20% n)	0.0134	0.03130	0.03130	0.02474	0.00787	0.000001
(70% w, 30% n)	0.03	0.06795	0.06795	0.05812	0.0302	0.0077
(60% w, 40% n)	0.01862	0.07448	0.07448	0.06434	0.0371	0.0134
(50% w, 50% n)	0.148	0.0026	0.0026	0.00124	0.000005	0.002
(40% w, 60% n)	0.0988	0.02124	0.02124	0.01631	0.00831	0.0024
(30% w, 70% n)	0.0664	0.03071	0.03071	0.0247	0.0159	0.00837
(20% w, 80% n)	0.177	0.00204	0.00204	0.0008	0.0002	0.000016
(10% w, 90% n)	0.129	0.00642	0.00642	0.0092	0.0086	0.0063
RMSE	0.0637	0.02322	0.02322	0.01942	0.01074	0.0068

Table 3. RMSE scores in fractional abundance estimation for the considered methods.

5. CONCLUSIONS AND FUTURE RESEARCH

This paper has described a combined HNN/MLP neural network for estimating the concentration of nitrogen salts in turbid inland waters. The proposed neural model integrates the concepts of linear and nonlinear unmixing. In a first stage, a rough estimation of concentrations is accomplihed by HNN via linear spectral unmixing. This initial estimation is refined by MLP in a second step using nonlinear mixing concepts. Experimental results demonstrate that the combined HNN/MLP approach produces estimations which are more accurate in terms of RMSE than those produced by the standard linear mixture model or the HNN neural model alone. An important issue for successful application of the combined HNN/MLP model is the selection of an appropriate set of training samples for supervised learning. In this work, we use pure spectral signatures (derived by the AMEE endmember extraction algorithm) as training samples. We also explored the impact of using additional mixed signatures for training purposes. From our experiments, we can conclude that endmember signatures alone cannot provide an appropriate training set for the network, which also requires other types of training samples such as mixed signatures. Future work will be focused on validating the estimation results obtained for a ROSIS hyperspectral scene using available ground-truth. We will also carry out an investigation of four different types of pixels: pure pixel, mixed pixel, anomalous pixel and homogeneous pixel to investigate appropriate mechanisms to generate a set of good training samples for networks in mixed pixel classification in unsupervised fashion.

ACKNOWLEDGEMENT

Javier Plaza would like to acknowledge Prof. Chein-I Chang for his advice and suggestions during a research visit to Remote Sensing Signal and Image Processing Laboratory (RSSIPL) at University of Maryland, Baltimore County. Antonio Plaza would like to thank for support received from the Spanish Ministry of Education and Science (PR2003-0360 Fellowship).

REFERENCES

1. G. Candiani, C. Giardino, N. Strömbeck and E. Zilioli, "Imaging spectrometry to estimate chlorophyll-a in Lake Garda," *Third EARSel Workshop on Imaging Spectroscopy*, Herrsching, Germany, 2003.
2. A.M. Matthews, A.G. Duncan, R.G. Davison, "An assessment of validation techniques for estimating chlorophyll-a concentration from airbone multiespectral imagery," *International Journal of Remote Sensing*, vol. 22, pp. 429-447, 2001
3. S. Thiemann and H. Kaufmann, "Determination of chlorophyll content and tropic state of lakes using field spectrometer and IRS-IC satellite data in the Mecklenburg Lake District, Germany," *International Journal of Remote Sensing*, vol. 21, pp. 227-235, 2000.
4. H. Schiller and R. Doerffer, "Neural network for emulation of an inverse model operational derivation of Case II water properties from MERIS data," *International Journal of Remote Sensing*, vol. 20, pp. 1735-1746, 1999.

5. L. Gross, S. Thiria, R. Frouin and B.G. Mitchell, "Artificial neural networks for modeling the transfer function between marine reflectance an phytoplankcton pigment concentration," *Journal of Geophysical Research*, vol. 105, pp. 3483-3495, 2000.
6. D. Buckton, E. O'Mongain and S. Danaher, "The use of neural networks for the estimation of oceanic constituents based on the MERIS instrument," *Journal of Geophysical Research*, vol. 20, pp. 1841-1851, 1999.
7. P.Cipollini, G. Corsini, M. Diani and R. Grasso, "Retrieval of sea water optically active parameters from hyperspectral data by means of generalized Radial Basis Function Neural Network," *IEEE Transactions on Geoscience and Remote Sensing*, vol. 39, pp. 1508-1524, 2001
8. A. Plaza, P. Martinez, R. Perez and J. Plaza, "Spatial/spectral endmember extraction by multidimensional morphological operations," *IEEE Transactions on Geoscience and Remote Sensing*, vol. 40, pp. 2025-2041, 2002
9. C.-I Chang, *Hyperspectral imaging: spectral detection and classification*, Kluwer Academic/Plenum Publishers, New York, 2003.
10. J. Plaza, P. Martinez, R.M. Perez and A. Plaza, "Nonlinear neural network mixture models for fractional abundance estimation in AVIRIS hyperspectral images," *XIII NASA/Jet Propulsion Laboratory Airborne Earth Science Workshop*. Pasadena, CA, USA, 2004.
11. J. Plaza, A. Plaza, P. Martinez and R.M. Perez, "Nonlinear mixture models for analyzing laboratory simulated-forest hyperspectral data," *IX SPIE Image and Signal Processing for Remote Sensing*. Barcelona, Spain, 2003.
12. J. Plaza, C.-I Chang, P. Martinez and A. Plaza, "On the generation of training samples for neural network-based mixed pixel classification," submitted to *SPIE Defense and Security Symposium*, Orlando, FL, USA.
13. J. Plaza, A. Plaza, P.Martinez, R.M. Perez, "H-COMP: A tool for quantitative and comparative analysis of endmember identification algorithms," *IEEE International Geoscience and Remote Sensing Symposium*, Toulouse, France, 2003.